JOURNAL OF GUIDANCE, CONTROL, AND DYNAMICS
Vol. 18, No. 4, July–August 1995

Optimal Atmospheric Trajectory for Aerogravity Assist with Heat Constraint

Fayyaz A. Lohar,* Arun K. Misra,† and Dan Mateescu‡
McGill University, Montreal, Quebec H3A 2K6, Canada

In a previous paper, the authors addressed the problem of augmenting gravity assist by using planetary atmospheric maneuvering such that the heliocentric velocity of the spacecraft after flyby was maximized. The optimization was carried out by using Pontryagin's maximum principle. The results showed that the heating rate was high during maneuvering of the spacecraft through the atmosphere. Therefore in the present paper, a heating rate constraint is imposed on the atmospheric trajectory for aerogravity assist (AGA). A comparison of AGA for Venus and Mars is given that shows the overall superiority of using Mars over Venus. The results also show that AGA with heat constraint gives slightly lower heliocentric velocity than AGA without heat constraint, particularly when the drag polar based on the Newtonian theory for the hypersonic regime is used in numerical calculations. This study concludes that AGA is possible with moderate planetocentric velocity.

Introduction

IN 1962 London[1] presented a paper in which he demonstrated the possibility of using atmospheric maneuvering to produce an appropriate aerodynamic force to change the spacecraft's terrestrial orbit with significantly smaller expenditure than an extra-atmospheric propulsive maneuver. Since then, several studies of aeroassisted orbit transfer (AOT) have been conducted for a wide variety of terrestrial orbits as well as planetary missions.[2] In these studies, the atmosphere was used either to reduce the velocity or to change the plane of the trajectory of the spacecraft, which leads to a change of its orbit when it emerges out of the atmosphere. On the other hand, Randolph and McRonald[3,4] proposed to use planetary atmospheric maneuvering to augment planetary gravity assist. This technique is called aerogravity assist (AGA).

Many solar system exploration missions (e.g., Voyager, Galileo) have used planetary gravity assist. The concept is based on the fact that energy can be transferred from or released to a planet's gravity field when a spacecraft's heliocentric trajectory is perturbed and deflected due to the gravitational attraction of the planet. This eventually changes the magnitude and direction of the spacecraft's heliocentric velocity V_s.[5] However, most planets (except Jupiter and Saturn) produce only a small ΔV (increase or decrease in V_s). That is why Galileo used multiple gravity assists (VEEGA) to reach Jupiter.[6] Missions to remote planets or solar flybys need either Jupiter gravity assist or other techniques such as AGA.

In AGA, a spacecraft enters the atmosphere of the planet and uses the aerodynamic lift force appropriately, in addition to the gravitational pull of the planet, to increase the rotation around the planet, thereby enhancing the gravity assist on the spacecraft. This is demonstrated in Fig. 1 in which the spacecraft enters the planetary atmosphere at point A, maneuvers for some time to increase the rotational angle, and leaves the atmosphere at point B. To limit the kinetic energy loss of the spacecraft during atmospheric maneuvering, the total drag must be small, which also implies a high L/D (lift-to-drag) ratio. With the possible advent of novel hypersonic vehicles (e.g., waverider), which have high L/D, a large deflection angle δ is possible. This can lead to quite a large ΔV and change in the direction of the heliocentric velocity V_s of the spacecraft.

Received May 19, 1994; revision received Dec. 5, 1994; accepted for publication Dec. 18, 1994.

*Graduate Student, Department of Mechanical Engineering. Member AIAA.

†Professor, Department of Mechanical Engineering. Associate Fellow AIAA.

‡Associate Professor, Department of Mechanical Engineering. Senior Member AIAA.

Earlier studies on AGA[3,4,7,8] have used simple analytical models and assumed a circular atmospheric trajectory. A recent study[9] by the authors presented a more realistic mathematical model and obtained an optimal atmospheric trajectory to maximize ΔV. The heating rates (convective and radiative) were also calculated, but the optimization was carried out without putting any constraint on heating rates, which were later found to be substantial (from 700 to 1200 W/cm^2, depending on the planetocentric velocity). Furthermore, only Venus was considered for AGA.

In the present paper, the analysis is made more realistic by imposing a heating rate constraint on the atmospheric trajectory. A comparison of ΔV for gravity assist and AGA with or without a heating rate constraint is carried out for different system parameters. Both Venus and Mars are considered for AGA.

The assumptions in our analysis are as follows. The vehicle has a lifting configuration, and the lift can be modulated by varying the angle of attack. Lift modulation is the sole means of controlling the flight-path angle in the atmosphere. Furthermore, the atmospheric properties, the vehicle's aerodynamic properties, the equations of motion, and the initial position and velocity of the vehicle are all known precisely. Finally, the heliocentric orbits of the planets are assumed to be coplanar and circular.

The basic events of an AGA mission are as follows. The spacecraft is launched from Earth orbit with a tangential thrust in the direction of the orbital velocity, which injects the vehicle in a heliocentric elliptical transfer orbit in such a way that it arrives at the planet with a planetocentric velocity V_∞^- at sufficiently far away distance (i.e., at a distance close to the limit of the planet's sphere of influence). The spacecraft approaches the planet along a hyperbolic trajectory H_{T1} with its periapsis located inside the atmosphere of the planet. At point A in Fig. 1b, the vehicle enters the atmosphere. It flies along an optimal trajectory with minimum loss of kinetic energy using modulated lift for maneuvering. In the case of AGA with heat constraint, the heating rate at the stagnation region should not exceed the prescribed heating rate constraint during maneuvering through the atmosphere. When it exits from the atmosphere (at point B), the path deflection angle δ has been sufficiently increased, whereas due to the loss of kinetic energy, V_∞^+ (V_∞ after AGA) is slightly less than V_∞^-. The spacecraft now follows a new hyperbolic trajectory H_{T2}. The flight-path angle, angle of rotation of the spacecraft through the atmosphere, and planetocentric velocity at B are optimized so as to give the maximum heliocentric velocity at a point on H_{T2} sufficiently far from the planet.

Equations of Motion

The equations of motion for planar atmospheric flight are[10]

$$\frac{dr}{dt} = V \sin\gamma \tag{1a}$$

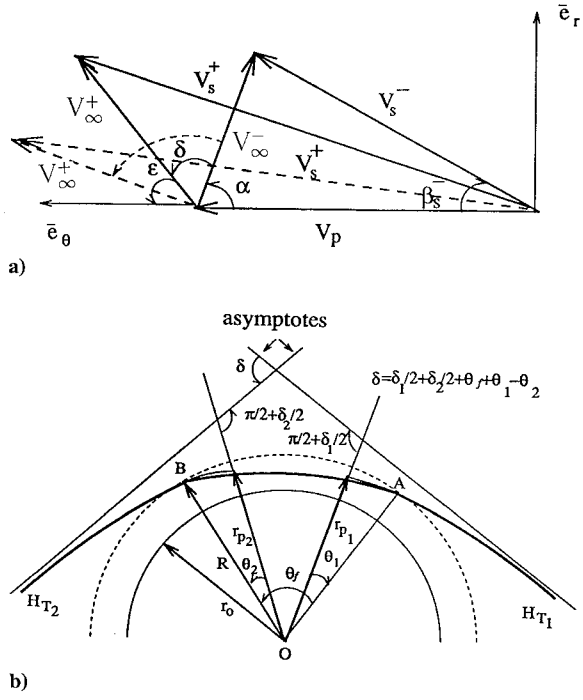

Fig. 1 a) Vector diagram of velocities: V_s^- and V_∞^- before gravity assist and aerogravity assist (– –), V_s^+ and V_∞^+ after gravity assist (— —), and after aerogravity assist (- - -); b) geometry of aerogravity assist trajectory.

$$\frac{d\theta}{dt} = \frac{V\cos\gamma}{r} \tag{1b}$$

$$\frac{dV}{dt} = -\frac{V^2\rho SC_D}{2m} - \frac{\mu}{r^2}\sin\gamma \tag{1c}$$

$$\frac{d\gamma}{dt} = \frac{V\rho SC_L}{2m} - \left(\frac{\mu}{Vr^2} - \frac{V}{r}\right)\cos\gamma \tag{1d}$$

where t is time, r is the radial distance between the spacecraft and the center of the planet, θ is the angle of planetocentric rotation of the spacecraft during maneuvering through the atmosphere of the planet, V is the velocity of the spacecraft, γ is the flight-path angle for planetocentric trajectory, μ is the gravitational constant multiplied by the mass of the planet, ρ is atmospheric density, S is the surface area of the spacecraft, and C_L and C_D are aerodynamic lift and drag coefficients related to the lift and drag forces acting on the spacecraft, respectively. It is assumed here that the planetary atmosphere is not rotating and atmospheric density varies exponentially with the altitude. Also, when $r > R$, where R is the radius of the sensible atmosphere (see Fig. 1b), the flight is Keplerian.

The drag polar used in the analysis is of the form[10]

$$C_D = C_{D0} + KC_L^n \tag{2}$$

where C_{D0} is the drag at zero C_D. In general, K and n are functions of the Mach number and the Reynolds number. At high Mach numbers, however, K and C_{D0} are almost independent of the Reynolds number (in laminar regime)[10,11]; since that is the case in the major part of the atmospheric trajectory here, we will assume K and C_{D0} to be constant. Moreover, from the drag polar we have the following useful relationships:

$$C_D^* = \left(\frac{C_{D0}}{(n-1)K}\right)^{1/n} \tag{3a}$$

$$E^* = \frac{C_L^*}{C_D^*} = \frac{1}{n}\left(\frac{1}{K}\right)^{1/n}\left(\frac{n-1}{C_{D0}}\right)^{(n-1)/n} \tag{3b}$$

where E^* is the maximum value of L/D and C_L^* and C_D^* are the corresponding values of C_L and C_D, respectively. Now one can introduce a new variable, $\lambda = C_L/C_L^*$; this is a normalized lift coefficient. In the following analysis λ will be used as an aerodynamic control parameter.

Although the drag polar is being used for the first time for AGA here, it has been used earlier in AOT and re-entry problems.[12,13] These investigators often used a parabolic drag polar ($n = 2$). However, a parabolic drag polar is basically valid for the subsonic regime, although some experimental results show its validity in the supersonic and low hypersonic regimes as well.[10,14] The velocity of the vehicle in the present case will be higher than these, because the planetocentric trajectory of the vehicle is hyperbolic, and hence the exponent value $n = 1.5$ will be used in the drag polar at high hypersonic velocities, as indicated by several authors based on Newtonian theory for hypersonic flows.[15] Newtonian theory is valid for both slender and blunt bodies at very high Mach numbers when the ratio of specific heats c_p/c_v becomes close to 1 due to ionization caused by high temperature.[15] However, since there are no experimental results available at very high velocities, results using both $n = 2$ and $n = 1.5$ are obtained in this paper for comparison purposes.

Using C_L or λ as a control parameter corresponds physically to using pitch modulation to shape the trajectory. In this paper C_L is allowed to assume both positive and negative values. A negative C_L value can be interpreted as resulting either from a negative pitch angle or from a positive angle with the vehicle flying upside down.

The independent variable is now changed from t to θ, because that makes it easier to handle the optimization problem. One then has to solve three equations instead of four, whereas θ can be included in the performance index, as will be seen later. The equations of motion in nondimensionalized form with θ as the independent variable are given below for the planar case:

$$\frac{dh}{d\theta} = h\tan\gamma \tag{4a}$$

$$\frac{dv}{d\theta} = -\frac{A\eta f(n,\lambda)vh}{E^*\cos\gamma} - \frac{b\tan\gamma}{hv} \tag{4b}$$

$$\frac{d\gamma}{d\theta} = \frac{Ah\eta\lambda}{\cos\gamma} + 1 - \frac{b}{v^2h} \tag{4c}$$

By using Eqs. (3) we have $f = \frac{1}{2}(1+\lambda^2)$ and $\frac{1}{3}(1+2|\lambda|^{1.5})$ for $n = 2$ and $n = 1.5$, respectively. The dimensionless variables and parameters used in Eq.(4) are defined as follows:

$$h = \frac{r}{r_0}, \qquad v = \frac{V}{\sqrt{\mu/R}}, \qquad b = \frac{R}{r_0}$$

$$\eta = \frac{\rho}{\rho_0} = e^{-z(r-r_r)}, \qquad z = \frac{1}{S_h}, \qquad A = \frac{\rho_0 S r_0 C_L^*}{2m}$$

where r_0 is the radius of the planet, m the mass of the spacecraft, S_h a scale height, $r_r - r_0$ the reference altitude for the density model, and ρ_0 the density at the reference altitude.

Heating Rate Constraint

During the flight of the spacecraft in the planetary atmosphere its kinetic energy decreases. A fraction of this energy is converted into heat absorbed by the vehicle. Here it will be assumed that only the highest temperature in the stagnation region of the vehicle is of concern. To control this temperature, it suffices to control the heating rate in that region. Moreover, if we impose a constraint on the heating rate, then the integrated heat load will automatically be reduced, although it may not be minimal.

The convective heating rate q_c along the atmospheric trajectory is computed according to the equation[15]

$$q_c = \frac{k\rho^{\frac{1}{2}}V^3}{(r_n)^{\frac{1}{2}}} \tag{5}$$

where r_n is the radius of the stagnation region and k is a constant dependent on the composition of the atmosphere. In the numerical calculations, the AGAs of Venus and Mars have been considered, whose atmospheres are assumed to contain 85% CO_2 and 15% N_2

(in reality, the atmospheres of Venus and Mars contain, respectively, 90% CO_2, 10% N_2 and 95% CO_2, 5% N_2, but the values of k for 90/10 and 95/5 mixtures are not available in the literature; in any case, k is not very sensitive to the mixture ratio). The value of k for the 85/15 mixture is taken from Ref.16, which is 1.8425×10^{-8} (which is likely to be close to the real values; note that even for 50/50 mixture, $k = 1.7765 \times 10^{-8}$). The above value of k assumes that q_c is in watts per square centimeter, ρ in kilograms per cubic meter, V in meters per second, and r_n in meters.

The radiative heating rate is computed according to the equation given in Ref. 17, i.e.,

$$q_r = F r_n^a \rho^p f(V) \tag{6}$$

where the $f(V)$ are tabulated values that are functions of flight velocity V and the atmospheric composition. The exponents a and p are functions of ρ and V. According to Page and Woodward,[18] at high velocities (e.g., 10 km/s) the radiative heating rate is more or less the same for the atmospheres of Earth, Venus, and Mars. The velocities of spacecraft in the present case will be higher than the above velocity. Actually, at a very high Mach number the atmospheric gases dissociate and become a partial ionized plasma, and the radiative heating rate for Earth, Venus, and Mars become approximately equal. Therefore the following values, which are for air, are used:

$$\begin{gathered} F = 4.736 \times 10^4 \\ a = 1.072 \times 10^6 V^{-1.88} \rho^{-0.325}, \qquad p = 1.22 \end{gathered} \tag{7}$$

In Eqs. (6) and (7), again the heating rate is in watts per square centimeter, ρ in kilograms per cubic meter, V in meters per second, and r_n in meters. The nose radius r_n has been taken as 0.5 and 1 m (Randolph and McRonald have used $r_n = 1$ m in Ref. 3 and in the studies on AOT mission r_n is taken as 1 m as well). Since only the heating rate range is of concern here, these models will suffice.

Now one has to decide which heating rate to select in the optimization problem for the heating rate constraint. Our calculations show that at low altitudes q_r will be much higher than q_c, but at high altitudes q_r is much lower than q_c. Since the altitude of maneuvering of the spacecraft in the present case will be high, q_c is selected to be used in the heating rate constraint.

Variational Formulation

Let V_s^+ be the final heliocentric velocity of the spacecraft after completing the maneuvering inside the atmosphere through an angle θ_f. The objective is to maximize V_s^+ subject to differential constraints represented by the equations of motion and the heating rate constraint. Thus one can define the performance index

$$J = V_s^+ \tag{8}$$

subjected to constraints represented by the equations of motion [Eq. (4)]. In addition, the heating rate constraint $q_c \leq q_{c,\max}$ can be included either in the optimization problem analytically or numerically depending on the type of problem.

Referring to Fig. 1a, the value of V_s^+ is given by

$$V_s^+ = \left(V_\theta^2 + V_r^2\right)^{\frac{1}{2}} \tag{9}$$

where

$$\begin{gathered} V_\theta = V_p + V_\infty^+ \cos\epsilon, \qquad V_r = V_\infty^+ \sin\epsilon \\ \epsilon = \pi - \alpha - \delta, \qquad V_\infty^+ = \left(V_f^2 - \frac{2\mu}{R}\right)^{\frac{1}{2}} \end{gathered} \tag{10}$$

The subscript f stands for the final value of a variable at the completion of the maneuvering of the spacecraft through the atmosphere. Furthermore, α is the angle between V_p (heliocentric velocity of the planet)and V_∞^- (Fig. 1a). The last equation in Eqs. (10) can be written in dimensionless form as

$$v_\infty^+ = \left(v_f^2 - 2\right)^{\frac{1}{2}} \tag{11}$$

where all the velocities have been divided by $(\mu/R)^{\frac{1}{2}}$.

From Figs. 1a and 1b, one can obtain

$$\delta = \tfrac{1}{2}\delta_1 + \tfrac{1}{2}\delta_2 + \theta_f + \theta_1 - \theta_2 \tag{12}$$

where

$$\theta_i = \tan^{-1}\left(\frac{v_i^2 \sin\gamma_i \cos\gamma_i}{v_i^2 \cos^2\gamma_i - 1}\right) \tag{13a}$$

$$\delta_i = 2\sin^{-1}(1/e_i) \tag{13b}$$

$$e_i = \left[\left(v_i^2 - 1\right)^2 \cos^2\gamma_i + \sin^2\gamma_i\right]^{\frac{1}{2}} \tag{13c}$$

where $i = 1, 2$. Subscripts 1 and 2 denote quantities for hyperbolic planetocentric trajectories H_{T1} and H_{T2} at A and B, respectively. Here, θ_1 and θ_2 are the angles between their hypothetical closest approaches r_{p1} and r_{p2} and lines AO and BO, respectively, as shown in Fig. 1b. In several previous studies θ_1 and θ_2 were assumed to be zero. However, for more accurate results these quantities should be included in the calculations.

At the entry point we have

$$\theta_e = 0, \qquad h_e = R/r_0 \tag{14}$$

and at the exit we have θ_f unspecified and

$$h_f = R/r_0 \tag{15}$$

Now the necessary conditions for optimal solution using Pontryagin's maximum principle are derived. Introducing the adjoint vector $\boldsymbol{p} = \{p_h, p_v, p_\gamma\}^T$ to form the Hamiltonian,[12] one obtains, for $n = 2$,

$$\begin{aligned} \mathcal{H} = {} & p_h h \tan\gamma + p_v\left(\frac{-A\eta v h(1+\lambda^2)}{2E^* \cos\gamma} - \frac{b\tan\gamma}{vh}\right) \\ & + p_\gamma\left(\frac{Ah\eta\lambda}{\cos\gamma} + 1 - \frac{b}{hv^2}\right) \end{aligned} \tag{16}$$

The optimal lift control corresponds to $d\mathcal{H}/d\lambda = 0$ and it gives

$$\lambda = \frac{E^* p_\gamma}{v p_v} \tag{17}$$

The components of $\boldsymbol{p}$ are governed by the adjoint equations

$$\frac{dp_x}{d\theta} = -\frac{\partial \mathcal{H}}{\partial x}, \qquad x = (h, v, \gamma) \tag{18}$$

Let us now introduce a new variable $C = p_h/p_v$. Then the new adjoints λ and C are governed by the system of differential equations

$$\begin{aligned} \frac{d\lambda}{d\theta} = {} & \frac{-E^* hC}{v\cos^2\gamma} + \frac{A\eta h \sin\gamma(1-\lambda^2)}{2\cos^2\gamma} + \frac{E^* b}{hv^2\cos^2\gamma} \\ & + \frac{2\lambda b\tan\gamma}{hv^2} + \frac{2\lambda^2 b}{E^* hv^2} \end{aligned} \tag{19}$$

$$\begin{aligned} \frac{dC}{d\theta} = {} & \frac{A\eta v(1-\lambda^2)(1-hr_0 z)}{2E^*\cos\gamma} - \frac{b\tan\gamma}{h^2 v} - C\tan\gamma - \frac{\lambda b}{E^* h^2 v} \\ & - \frac{A\eta hC(1+\lambda^2)}{2E^*\cos\gamma} + \frac{Cb\tan\gamma}{hv^2} + \frac{2Cb\lambda}{E^* hv^2} \end{aligned} \tag{20}$$

One can now obtain the modified Hamiltonian in terms of λ and C as

$$\hat{\mathcal{H}} = \frac{A\eta v h(\lambda^2 - 1)}{2E^*\cos\gamma} - \frac{b\tan\gamma}{hv} + \frac{\lambda v}{E^*} - \frac{\lambda b}{E^* hv} + Ch\tan\gamma \tag{21}$$

If n is taken as 1.5 in the drag polar instead of 2, then Eqs. (19–21) become

$$\frac{d\lambda}{d\theta} = -\frac{2E^*hC|\lambda|^{\frac{1}{2}}}{v\cos^2\gamma} + \frac{2A|\lambda|^{\frac{1}{2}}\eta h\sin\gamma\left(1-|\lambda|^{\frac{3}{2}}\right)}{3\cos^2\gamma} + \frac{2|\lambda|^{\frac{1}{2}}E^*b}{hv^2\cos^2\gamma} + \frac{4\lambda b\tan\gamma}{hv^2} + \frac{4|\lambda|^{\frac{3}{2}}b}{E^*hv^2} \tag{22}$$

$$\frac{dC}{d\theta} = \frac{A\eta v\left(1-|\lambda|^{\frac{3}{2}}\right)(1-hr_0z)}{3E^*\cos\gamma} - \frac{b\tan\gamma}{h^2v} - C\tan\gamma - \frac{|\lambda|^{\frac{1}{2}}\operatorname{sgn}(\lambda)b}{E^*h^2v} - \frac{A\eta hC\left(1+2|\lambda|^{\frac{3}{2}}\right)}{3E^*\cos\gamma} + \frac{Cb\tan\gamma}{hv^2} + \frac{2Cb|\lambda|^{\frac{1}{2}}\operatorname{sgn}(\lambda)}{E^*hv^2} \tag{23}$$

$$\hat{\mathcal{H}} = Ch\tan\gamma - \frac{A\eta vh\left(|\lambda|^{\frac{3}{2}}+1\right)}{3E^*\cos\gamma} - \frac{b\tan\gamma}{hv} + \frac{|\lambda|^{\frac{1}{2}}\operatorname{sgn}(\lambda)v}{E^*} - \frac{|\lambda|^{\frac{1}{2}}\operatorname{sgn}(\lambda)b}{E^*hv} + \frac{A\eta hv\lambda|\lambda|^{\frac{1}{2}}\operatorname{sgn}(\lambda)}{E^*\cos\gamma} \tag{24}$$

Since the final value of θ is unspecified, the optimal solution needs a set of transversality conditions to be satisfied, since a functional or performance index that is dependent on the final values of the state variables is being maximized. These conditions are

$$p_{\theta_f} = \frac{\partial J}{\partial\theta_f}, \qquad p_{v_f} = \frac{\partial J}{\partial v_f}, \qquad p_{\gamma_f} = \frac{\partial J}{\partial\gamma_f} \tag{25}$$

From Eq. (17), then, the transversality condition to be satisfied by the normalized lift coefficient is

$$\lambda_f = E^*p_{\gamma_f}/v_fp_{v_f}, \qquad \text{for} \qquad n=2 \tag{26}$$

and

$$|\lambda_f| = \left(E^*p_{\gamma_f}/v_fp_{v_f}\right)^2 \qquad \text{for} \qquad n=1.5 \tag{27}$$

where

$$p_{v_f} = \frac{v_f(v_\theta\cos\epsilon + v_r\sin\epsilon)}{v_sv_\infty^+} + \frac{\partial\delta}{\partial v_f}\frac{v_\infty^+(v_\theta\sin\epsilon - v_r\cos\epsilon)}{v_s} \tag{28a}$$

$$p_{\gamma_f} = \frac{v_\infty^+(v_\theta\sin\epsilon - v_r\cos\epsilon)}{v_s}\frac{\partial\delta}{\partial\gamma_f} \tag{28b}$$

$$p_{\theta_f} = \frac{v_\infty^+(v_\theta\sin\epsilon - v_r\cos\epsilon)}{v_s} \tag{28c}$$

The values of $\partial\delta/\partial v_f$ and $\partial\delta/\partial\gamma_f$ are quite lengthy and are therefore omitted for brevity. The quantities δ, ϵ, etc., are shown in Fig. 1a. Note that the final value of the independent variable is included in the performance index; hence $\hat{\mathcal{H}} \neq 0$.[12] Therefore the modified Hamiltonian $\hat{\mathcal{H}}$ satisfies the second transversality condition

$$\hat{\mathcal{H}}_f - p_{\theta_f}/p_{v_f} = 0 \tag{29}$$

Now there are five differential equations, namely Eqs. (4) for the three states and either Eqs. (19) and (20) or (22) and (23), depending on n. Integration of these equations will yield extremal trajectories for a number of situations that differ only in the entry and exit conditions that need to be satisfied. Here, we have a two-point boundary value problem, since the states satisfy specified conditions at $\theta = 0$, whereas h and the costates p_v, p_γ must satisfy conditions specified at $\theta = \theta_f$. The problem is also a two-parameter problem because $\hat{\mathcal{H}} \neq 0$, and we have to guess the initial values of C and λ during the course of solving the two-point boundary value problem. The accuracy of numerical integration is checked by examining the Hamiltonian $\mathcal{H}$, which must be constant.

Method of Numerical Solution

Calculations are carried out with a specified value of V_∞^-. Different values of V_∞^- imply different heliocentric trajectories from Earth to the planet. From these, the entrance conditions v_e and γ_e can be computed. The two-point boundary value problem resulting from the optimization is solved by the shooting method. Let us first consider the optimization problem without any heating rate constraint. Using the computed values of v_e and γ_e, setting $h_e = R/r_0$, and choosing initial guesses for λ_e and C_e as initial conditions, Eqs. (4), (19), and (20) or (4), (22), and (23) are integrated from $\theta = 0$ until h becomes R/r_0 again. The integration is performed using the Admas–Moulton method up to order 12, with local absolute error controlled to be less than 1.0×10^{-8}. In all the cases studied, it has been possible to find a set of initial guesses of λ_e and C_e such that the boundary conditions are satisfied at the exit. The increase in r_{p1} does not affect the atmospheric trajectory much, except that λ_e increases.

The trajectory and control computed are optimal, since the necessary conditions [Eqs. (4), (19), and (20)], the entry and exit conditions [Eqs. (14) and (15)], and the transversality conditions [Eqs. (26) and (29)] are satisfied. There is more than one local maximum, but the global maximum can be identified by examining the atmospheric trajectory. For example, for the optimal solution without heat constraint, in the case of global maximum, θ_f must be significantly large and kinetic energy loss must be small; i.e., the vehicle should fly close to E^* during most of the atmospheric trajectory. It was noted that the tolerance in satisfying the exit boundary conditions has a negligible effect on the optimal value of V_s^+ due to the highly nonlinear behavior of the boundary conditions.

When a heating rate constraint is imposed, the solution procedure is somewhat different. Previous studies on skip trajectories show that the heating rate increases in a monotonic fashion, reaching its maximum value shortly after the atmospheric entry. It then decreases during the remainder of the flight. Mease and Vinh[19] have presented an approach to solve the heating rate constraint problem for a skip trajectory successfully. In this approach one begins at time zero, the goal being to choose λ_e such that at some time $q_c = q_{c_{\max}}$ and $\dot{q}_c = 0$. When this value is achieved, then, the second stage is to find the values of λ and C such that the boundary conditions are satisfied at the atmospheric exit. We tried to use this approach in our case, but after solving the first part, i.e., $q_c = q_{c,\max}$ and $\dot{q}_c = 0$, we found that convergence for the second part was possible only when the altitude reduced to that corresponding to the maximum L/D ratio and the heating rate constraint was violated. Hence, we concluded that this approach is difficult to implement for highly nonlinear boundary conditions.

Therefore, another approach, similar to the one used by Chern and his colleagues in Ref. 20, was used in solving our optimization problem with heating rate constraint. In this approach, the boundary conditions remain the same; however, the problem is solved in parts. In the first part, we begin at $\theta = 0$, as in the case of the unconstrained optimization, except that now the aim is to choose λ_e such that

$$q_c = q_{c,\max}, \qquad \frac{d\gamma}{d\theta} = 0, \qquad \gamma = \gamma_c < 0, \qquad \theta = \hat{\theta}_1 \tag{30}$$

where γ_c is a specified flight-path angle. In the second part, γ remains constant, equal to γ_c, along the trajectory over an interval of specified θ ($\hat{\theta} = \hat{\theta}_1 - \hat{\theta}_2$). The selection of γ_c is made in such a way that the spacecraft maneuvers close to the boundary of $q_{c,\max}$. The value of $\hat{\theta}$ is determined by iteration. At some point where $\theta = \hat{\theta}_2$, the spacecraft leaves the γ_c trajectory and moves along a third trajectory, for which we choose C such that the boundary conditions are satisfied at the radius of the sensible atmosphere. Thus, the function C is discontinuous at $\hat{\theta}_1$, although the states h, v, γ and the adjoint λ are always continuous. (Note that the control law is changed to $\lambda = [b/(v^2h) - 1]\cos\gamma/A\eta h$ during the interval $\hat{\theta}$, and C is not used to calculate λ.)

Table 1 Comparison of Mars AGA and Venus AGA results with V_∞^-

Parameters	Mars results			Venus results		
	$V_\infty^- = 10.00$ km/s	$V_\infty^- = 12.00$ km/s	$V_\infty^- = 14.00$ km/s	$V_\infty^- = 10.00$ km/s	$V_\infty^- = 12.00$ km/s	$V_\infty^- = 14.00$ km/s
V_∞^+, km/s	7.72	9.15	10.60	8.31	9.34	10.83
V_s^-, km/s	25.32	26.84	28.46	36.20	35.54	34.83
V_s^+, km/s	31.65	33.20	34.69	43.14	44.23	45.58
V_s^+ (GA), km/s	27.31	28.47	29.76	42.03	41.36	40.37
$\frac{1}{2}\delta_1$, deg	6.36	4.57	3.44	20.23	15.57	12.25
$\frac{1}{2}\delta_2$, deg	9.95	7.41	5.73	25.70	22.17	18.10
θ_f, deg	83.94	89.15	93.40	46.75	63.48	69.21
β_s^-, deg	23.25	26.62	29.42	16.10	19.53	23.09
β_s^+, deg	3.72	2.53	2.16	2.86	2.45	3.60
ΔV_E, km/s	4.51	5.04	5.72	4.14	4.51	5.04
r_{a_s}, 10^9 km	2.72	7.45	∞	0.67	0.84	1.12
λ_e	0.32	−0.33	2.40	3.02	1.93	0.59
γ_e, deg	−9.00	−9.00	−10.00	−6.00	−6.00	−6.00
For $r_n = 1$ m						
$q_{c,\max}$, W/cm^2	223.65	351.43	586.78	361.47	464.71	611.45
$q_{r,\max}$, W/cm^2	18.10	356.01	816.42	272.23	398.37	523.00
For $r_n = 0.5$ m						
$q_{c,\max}$, W/cm^2	316.29	497.00	829.83	511.20	657.20	864.72
$q_{r,\max}$, W/cm^2	12.38	244.85	561.51	187.23	274.00	359.70

Numerical Results and Discussion

For the cases below, the planet for AGA was chosen as either Venus or Mars. Thus the heliocentric trajectory of the spacecraft is changed at the distance of 1.084×10^8 or 2.27×10^8 km from the sun for Venus or Mars, respectively, i.e., at the mean distance of Venus or Mars from the sun. The radius of the sensible atmosphere, R is taken as 6190 and 3483 km for Venus and Mars, respectively (the radius of Venus is 6050 km and that for Mars is 3383 km). It has been observed in other problems that a variation in the radius of the sensible atmosphere R does not affect the atmospheric trajectory much.[19] Above this altitude, the atmospheric density is assumed to be identically zero. Within the assumed atmospheric flight altitude range, i.e., 40–140 km for Venus and 20–100 km for Mars, the density is approximated by a model in which the density reduces exponentially with the increase in altitude. The scale height S_h, defined earlier, is selected according to the atmospheric data of Venus and Mars given in Refs. 21 and 22. It is assumed that $m/C_{L,\max}S = 50$ kg/m^2 for all the cases ($C_{L,\max}$ stands for maximum C_L at the stalling angle of attack), which is the same as that used by Randolph and McRonald.[3,4]

The results of the analysis are presented in three parts: 1) comparison of V_s^+ and other parameters obtained from simple gravity assist (GA) with optimal AGA from Venus and Mars; 2) comparison of the optimal trajectories without heat constraint for $n = 2$ (the cases without heat constraint for $n = 2$ and $n = 1.5$ are identified), with heat constraint for $n = 2$, and with heat constraint for $n = 1.5$; 3) comparison of V_s^+ and other parameters for the above three cases.

Comparison of GA and AGA for Venus and Mars

Three values of V_∞^- are chosen for analysis here, i.e., 10, 12, and 14 km/s. Corresponding values of V_s^+ with AGA are shown in Fig. 2 for the two planets along with the results for simple GA. It is assumed that the vehicle has $E^* = 5$ at hypersonic velocity. To obtain the results for GA, we have taken the closest approach r_p as 6550 and 3683 km for Venus and Mars, respectively, which are well above the radii of the corresponding atmospheres. It is clear from Fig. 2 that AGA in general is superior to simple GA for both cases. One might argue that the ΔV with GA is lower partly because the distance of closest approach is greater compared to AGA. However, this difference in r_p has only a negligible effect, as can be confirmed from Table 1. In this Table, V_s^+ for simple GA has been calculated using the same r_p as in AGA, assuming there is no atmosphere at those altitudes; the values of V_s^+ for simple GA here are very close to those in Fig. 2, obtained using the higher r_p.

Table 1 also presents some detailed results for AGA for three different values of V_∞^-. An important quantity listed in judging the effectiveness of AGA (or GA) is ΔV_E, which is the ΔV needed at a low Earth orbit to send the spacecraft to Venus and Mars to arrive with a given V_∞^-.

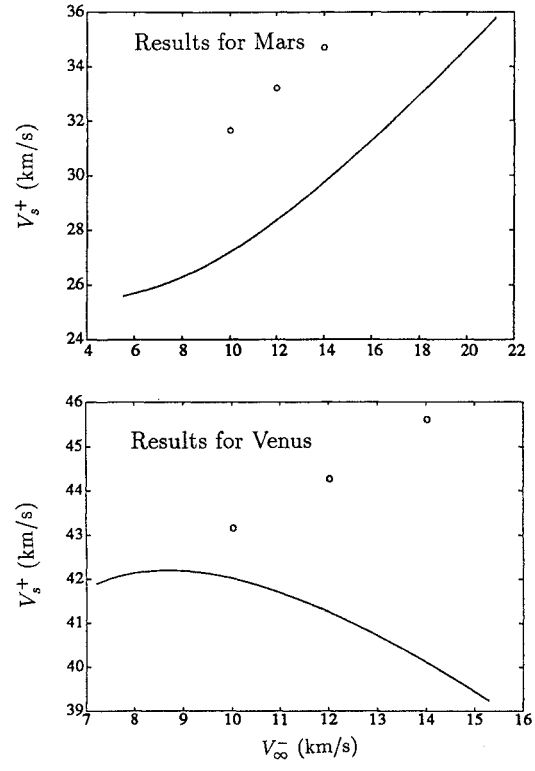

Fig. 2 Variation of V_s^+ vs V_∞^- for GA and AGA for Venus and Mars: o, AGA; solid line, GA.

It can be seen in Table 1 that δ_2 is greater than δ_1; this is due to the loss of kinetic energy of the spacecraft because of the drag during maneuvering through the planetary atmosphere. It also shows that θ_f for AGA increases with an increase in V_∞^- leading to greater V_s^+. This happens because the sum of δ_1 and α decreases with an increase in V_∞^-. Examining in Table 1 the values of the heliocentric flight-path angle β_s before and after AGA, it is clear that, after AGA, the perihelion after flyby is close to the planet. It may also be noted that λ_e decreases (while γ_e is constant) with increasing V_∞^-, which implies increasing entrance velocity V_e. This is logical because a

higher V_e needs less lift in the beginning to bring the spacecraft to an appropriate altitude for the maneuver.

Now the two planets are compared regarding the effectiveness of their AGA. For Venus, the difference between V_s^+ for AGA and GA decreases with a reduction in V_∞^-, because at smaller V_∞^-, e.g., $V_\infty^- <$ 10 km/s, $\cos\epsilon$ becomes close to 1 and there is not much benefit of AGA. Hence the AGA of Venus is advantageous only when $V_\infty^- \geq 10$ km/s. On the contrary, for Mars, the difference between V_s^+ for AGA and GA does not decrease much with a decrease in V_∞^-; this is because Mars has a significantly smaller mass than Venus. It can also be seen from Table 1 that the value of aphelion r_{a_s} after AGA is much higher for the case of Mars because of its farther location from the sun compared with Venus. Also, the heating rates for the case of Mars are much lower than those for Venus, because V_e is lower in the former case due to lower mass. Therefore, one can conclude that Mars is a more suitable candidate for AGA than Venus.

Nature of Atmospheric Trajectories with and Without Heat Constraint

Figure 3 shows the variation of v, γ, and h with θ for the optimal atmospheric trajectories for three cases: without heat constraint for $n = 2$ and with heat constraint for $n = 2$ as well as $n = 1.5$. Since in a previous paper[9] it was shown that the optimal atmospheric trajectories without heat constraint for $n = 2$ and $n = 1.5$ are nearly the same, only one case of optimal atmospheric trajectory without heat constraint is given here. Solid, dashed, and dash-dotted lines show the time history for the three cases: without heat constraint and with heat constraint for $n = 2$ and $n = 1.5$. The value of V_∞^- is taken as 12 km/s, the planet is Mars, and $E^* = 5$. The maximum heating rate constraint is chosen as 200 w/cm^2 for $r_n = 1$ m. Since we want to reduce the heating rate as much as possible, the spacecraft should fly at nearly maximum lift coefficient $\lambda_{\max}$ when $q_c = q_{c,\max}$, $d\gamma/d\theta = 0$, $\gamma = \gamma_c < 0$. Without heat constraint, we see that most of the time the vehicle stays close to $\lambda = -1$, as shown in Fig. 4, which means maximum $L/D = E^*$, to limit the loss of kinetic energy, and maintains a nearly constant γ close to zero. For the same case, the variation of h versus θ in Fig. 3 reveals that a few moments after the vehicle enters the atmosphere the altitude of the vehicle becomes nearly constant, which means that the vehicle flies in a close to circular path for some time and then leaves the atmosphere. As can be seen in Fig. 4, $\lambda = -1$ during this period.

The atmospheric trajectories for heat constraint cases with $n = 2$ and $n = 1.5$ are nearly identical, except for the variation of v vs θ, which is different for the two cases. Figure 3 shows that the final velocity for the $n = 1.5$ case is close to that without the heat constraint and higher than the $n = 2$ case. This is because the overall L/D during the atmospheric maneuvering is higher in magnitude for $n = 1.5$ compared to $n = 2$, as shown in Fig. 4. One can observe from Fig. 4 that the vehicle stays most of the time on the constant flight-path angle γ_c, which transforms the atmospheric trajectory to a spiral shape at the lower altitudes.

One may ask why one should not use a circular path instead of the spiral one (heating rate constraint case) in the lower altitude region of the atmospheric trajectory, as has been suggested in the earlier investigations. Results show that V_s^+ for a circular path will be lower than that for the spiral case, e.g., for $V_\infty^- = 12$ km/s and $n = 1.5$ for AGA with heat constraint, optimal V_s^+ is 33.00 km/s, whereas for a circular path $V_s^+ = 32.23$ km/s. After achieving the point when $q_c = q_{c,\max}$, $d\gamma/d\theta = 0$ in the atmosphere, for a circular path the altitude remains constant and q_c and $|\lambda|$ decrease with the reduction in the planetocentric velocity due to aerodynamic drag, whereas in the case of a spiral path q_c remains constant and $|\lambda|$ decreases further because of the decreasing altitude (increasing density) and drag. Thus $|\lambda|$ is lower in the case of a spiral path than that for the circular path, and this leads to a higher overall L/D, and as a result the planetocentric velocity is higher for AGA (heat constraint case) after maneuvering in the atmosphere through the same $\hat{\theta}$.

Figure 5 shows that the heating rate and dynamic pressure are much lower in the presence of a heat constraint. Without the heat constraint, the dynamic pressure reaches a peak value a few moments after the vehicle enters the atmosphere. Then it gradually decreases because of the loss of kinetic energy. On the other hand, with the heat constraint, the dynamic pressure, given by $p_d = \frac{1}{2}\rho V^2$, keeps on increasing in the lower altitude region of the atmospheric trajectory despite a decrease in velocity due to the drag; this happens because continuous decrease in altitude leads to increasing density. On the other hand, the expression for the heating rate contains the square root of the density ρ and cube of the planetocentric velocity V [see Eq. (5)]. Thus the heating rate depends mainly on V and not so much on ρ. This is the reason why continuously increasing density in the lower altitude region of the atmospheric trajectory with a slight decrease in V does not affect the heating rate significantly. Hence, we get a nearly constant heating rate.

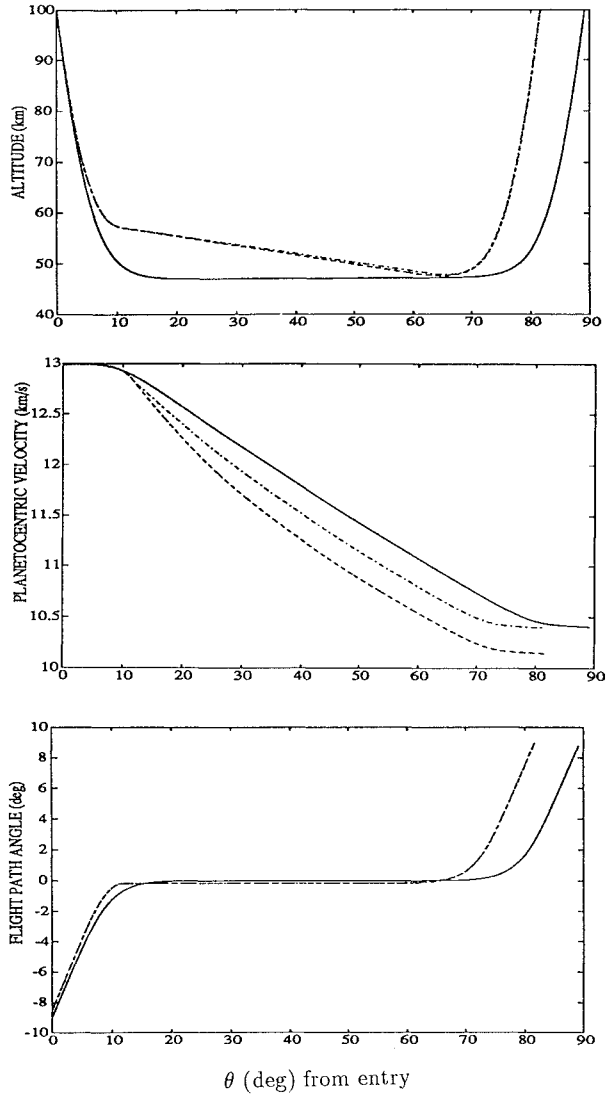

Fig. 3 Variation of state variables with θ: ——, without heat constraint; – – –, with heat constraint, $n = 2$; –·–, with heat constraint, $n = 1.5$.

Comparison of AGA for Cases Without and with Heat Constraint

Table 2 shows that V_s^+ for AGA with heat constraint and $n = 1.5$ is somewhat lower than that without heat constraint; V_s^+ for AGA with heat constraint and $n = 2$ is reduced even further. In all cases, $V_\infty^- = 12$ km/s. A larger V_s^+ with $n = 1.5$ compared to $n = 2$ (with heat constraint) is related to the former's superior overall L/D in the atmospheric trajectory. It was observed that in the absence of heat constraint, V_s^+ is more or less the same whether n is assumed to be 2 or 1.5. Furthermore, it can also be observed in Table 2 that for the all cases the difference in V_s^+, for $E^* = 5$ and $E^* = 7$, is substantial. This shows the significance of the maximum lift-to-drag ratio, E^* for any AGA mission.

One can also notice from Table 2 that γ_e is smaller in magnitude for AGA with heat constraint compared to that of AGA without heat constraint. This is because with the heat constraint a lower heating

Table 2 Variation of AGA results with E^*

	$E^* = 5$			$E^* = 7$		
Parameters	w/o hc	whc $n = 2$	whc $n = 1.5$	w/o hc	whc $n = 2$	whc $n = 1.5$
V_∞^+, km/s	9.15	8.85	9.14	9.72	9.37	9.69
V_s^-, km/s	26.84	26.84	26.84	26.84	26.84	26.84
V_s^+, km/s	33.20	32.72	33.00	33.72	33.38	33.66
θ_f, deg	89.15	81.47	81.36	99.21	86.58	86.34
β_s^-, deg	26.62	26.62	26.62	26.62	26.62	26.62
β_s^+, deg	2.53	4.37	4.58	2.23	3.21	3.50
For $r_n = 1$ m						
$q_{c,\max}$, W/cm^2	351	200	200	362	200	200
$q_{r,\max}$, W/cm^2	356	68	69	365	69	71
For $r_n = 0.5$ m						
$q_{c,\max}$, W/cm^2	497	283	283	512	283	283
$q_{r,\max}$, W/cm^2	245	47	47	251	47	49
$p_{d,\max}$, kN/m^2	7.05	4.43	4.50	7.07	4.50	4.61
Maximum g	4.25	4.50	4.50	4.30	4.53	4.53
r_{a_s}, 10^9 km	7.48	4.94	6.18	22.22	9.21	14.21
γ_c, deg	N/A	−0.175	−0.165	N/A	−0.130	−0.121
γ_e, deg	−9.00	−8.50	−8.50	−9.00	−8.50	−8.50

Note: w/o hc = AGA without heat constraint, whc = AGA with heat constraint, N/A = not applicable.

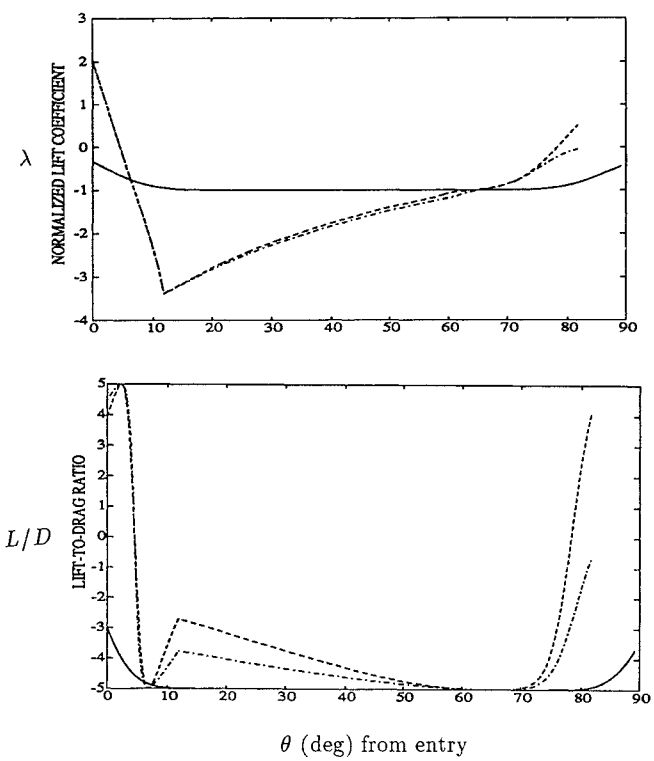

Fig. 4 Variation of normalized lift coefficient λ and lift-to-drag ratio L/D with θ: ——, without heat constraint; – – –, with heat constraint, $n = 2$; –·–, with heat constraint, $n = 1.5$.

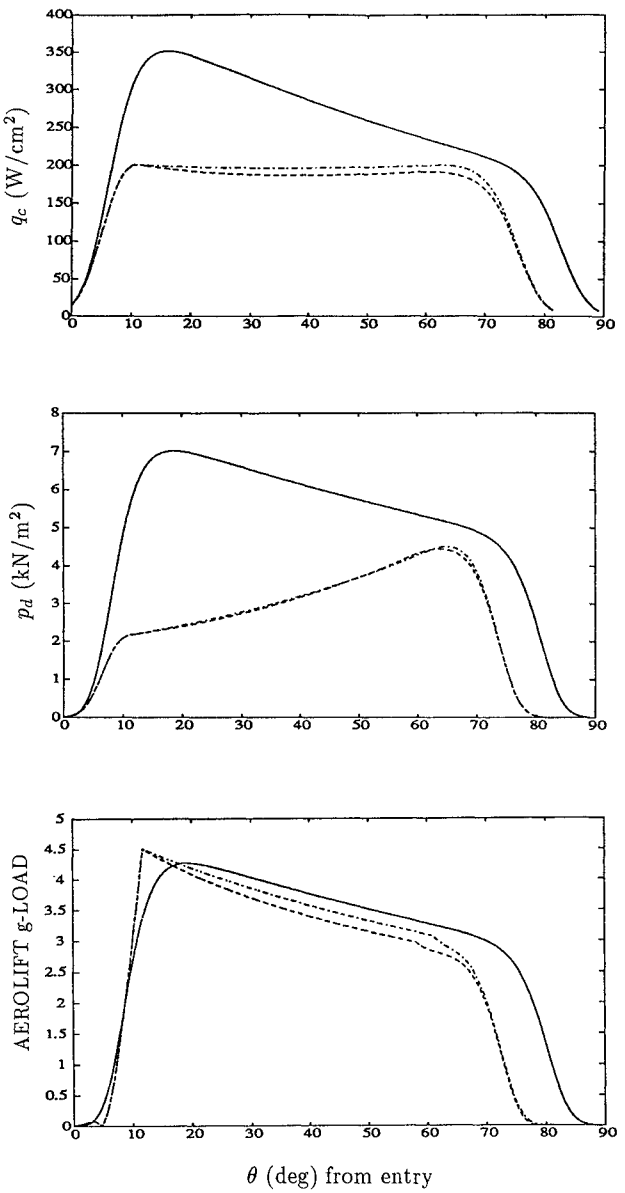

Fig. 5 Variation of convective heating rate q_c (for $r_n = 1$ m), dynamic pressure p_d, and aerolift g load with θ: ——, without heat constraint; – – –, with heat constraint, $n = 2$; –·–, with heat constraint, $n = 1.5$.

rate is desired that requires the spacecraft to have a higher periapsis; this means lower flight-path angle γ_e at atmospheric entry. Table 2 also shows that γ_c (i.e., the value of the flight-path angle in the second regime of the atmospheric maneuvering) for the $n = 1.5$ case is slightly smaller than that for the $n = 2$ case, because the overall L/D for $n = 1.5$ is superior to that for $n = 2$, as mentioned above, which implies less drag. Thus the lower magnitude of γ_c for $n = 1.5$ decreases the rate of decrease of altitude (i.e., the rate of increase of density) to maintain the constant heating rate.

It may be interesting to compare the dynamic pressures in AOT with that for AGA. As one can see in Table 2, for $V_\infty^- = 12$ km/s, the maximum dynamic pressure $p_{d,\max}$ associated with AGA with heat constraint is less than 5 kN/m^2, compared to 8.8 kN/m^2 for an AOT mission.[19] The maximum aerolift g load for AOT is 3.7, slightly lower than that for AGA (see Table 2). Though the heating

rate constraint considered for AOT in Ref.19 the term is 150 W/cm^2 (in Ref. 19 the term r_n is taken as 1 m), which is less than that for AGA (i.e., 200 W/cm^2 for $r_n = 1$ m), the time of atmospheric maneuvering of the spacecraft for AGA is substantially lower (67% less), resulting in a lower total heat load. This implies that an AGA mission for $V_\infty^- = 12$ km/s or less is possible if AOT can be executed.

Conclusion

Maximization of the heliocentric velocity of a spacecraft after AGA with constraints on the heating rate is considered. The problem has been formulated mathematically, and necessary conditions for optimal atmospheric trajectories and control have been derived for the cases of $n = 2$ and $n = 1.5$, i.e., parabolic drag polar and drag polar based on the Newtonian theory for the hypersonic regime. The optimization of the atmospheric trajectory with heat constraint is carried out successfully with a new approach. Comparison between the AGA trajectories with and without heat constraint tells us that V_s^+ (heliocentric velocity after AGA) is only slightly lower in the presence of the heat constraint, provided $n = 1.5$. One might point out that $n = 1.5$ is more appropriate than $n = 2$ at high hypersonic velocities. In the heat constraint case, the dynamic pressure is substantially smaller. In this study, the superiority of Mars over Venus for AGA was observed. In the case of Venus AGA is better than GA only when V_∞^- is greater than 10 km/s; the heating rates are then high. But this is not the case with Mars AGA. Although ΔV_E (i.e., velocity increment required at the low Earth orbit) is slightly less for Venus AGA than for Mars AGA, this advantage of Venus AGA cancels out when one looks at the values of aphelion for the two cases. In the case of Mars AGA, aphelion r_{a_s} is much bigger compared to Venus AGA because of the former's larger distance from the sun.

The detailed results of AGA with heat constraint show that AGA can be utilized even with today's technology. Comparison of AGA and AOT shows that the spacecraft for an AGA mission will need slightly more thermal shielding to avoid heating. Since it will not carry as big a payload as in the case of an OTV (orbit transfer vehicle), a slight increase in the weight of the spacecraft for shielding will not affect the mission. Furthermore, Mars AGA with moderate heating rates along with Jupiter GA can be used for solar flyby and Pluto missions.

Acknowledgments

The authors gratefully acknowledge support by the Natural Sciences and Engineering Research Council of Canada and the financial aid to the first author by the Ministry of Science and Technology of the Government of Pakistan.

References

[1]London, H. S., "Change of Satellite Orbit Plane by Aerodynamic Maneuvering," *Journal of the Aerospace Sciences*, Vol. 29, March 1962, pp. 323–332.

[2]Walberg, G. D., "A Survey of Aero-Assisted Orbit Transfer," *Journal of Spacecraft and Rockets*, Vol. 22, No. 1, 1985, pp. 3–18.

[3]Randolph, J. E., and McRonald, A. D., "Solar Probe Mission Status," presented at the AAS/GSFC International Symposium on Orbital Mechanics and Mission Design, Paper AAS 89-212, Washington DC, April 24–27, 1989.

[4]McRonald, A. D., and Randolph, J. E., "Hypersonic Maneuvering to Provide Planetary Gravity Assist," *Journal of Spacecraft and Rockets*, Vol. 29, No. 2, 1992, pp. 216–222.

[5]Kaplan, M. H., *Modern Spacecraft Dynamics and Control*, Wiley, New York, 1976.

[6]D'Amario, L. A., Byrnes, D. V., Johannesen, J. R., and Nolan, B. G., "Galileo 1989 VEEGA Trajectory Design," *Journal of the Astronautical Sciences*, Vol. 37, No. 3, 1989, pp. 281–306.

[7]Anderson, J. D., Lewis, M. J., and Kothari, A. P., "Hypersonic Waveriders for Planetary Atmospheres," *Journal of Spacecraft and Rockets*, Vol. 28, No. 4, 1991, pp. 401–410.

[8]Lewis, M. J., and Kothari, A. P., "Hypersonic Waverider for Planetary Maneuvering," presented at First International Hypersonic Waverider Symposium, Univ. of Maryland, College Park, MD, Oct. 17–19, 1990.

[9]Lohar, F. A., Mateescu, D., and Misra, A. K., "Optimal Atmospheric Trajectory for Aero-Gravity Assist," *Acta Astronautica*, Vol. 32, No. 2, 1994, pp. 89–96.

[10]Vinh, N. X., Buseman, A., and Culp, R. D., *Hypersonic and Planetary Entry Flight Mechanics*, Univ. of Michigan Press, Ann Arbor, MI, 1980.

[11]Miele, A., *Flight Mechanics*, Vol. 1: *Theory of Flight Paths*, Addison–Wesley, Reading, MA, 1966.

[12]Vinh, N. X., *Optimal Trajectories in Atmospheric Flight*, Elsevier Scientific, New York, 1981.

[13]Mease, K. D., "Optimization of Aeroassisted Orbital Transfer: Current Status," *Journal of the Astronautical Sciences*, Vol. 36, No. 1/2, 1988, pp. 7–33.

[14]Penlund, J. A., "Wall Temperature Effects on the Aerodynamics of a Hydrogen-Fueled Transport Concept in Mach 8 Blowdown and Shock Tunnels," NASA TP-2159, July 1983.

[15]Anderson, J. D., *Hypersonic and High Temperature Gas Dynamics*, McGraw–Hill, New York, 1989.

[16]Sutton, K., and Graves, R. A., Jr., "A General Stagnation Point Convective Heating Equation for Arbitrary Gas Mixtures," NASA TR-R376, Nov. 1971.

[17]Tauber, M. E., and Sutton, K., "Stagnation-Point Radiative Heating Relations for Earth and Mars Entries," *Journal of Spacecraft and Rockets*, Vol. 28, 1991, pp. 40–42.

[18]Page, W. A., and Woodward, H. T., "Radiative and Convective Heating During Venus Entry," *AIAA Journal*, Vol. 10, No. 10, 1972, pp. 1379–1381.

[19]Mease, K. D., and Vinh, N. X., "Minimum Fuel Aero-Assisted Coplanar Orbital Transfer Using Lift Modulation," *Journal of Guidance, Control, and Dynamics*, Vol. 8, No. 1, 1985, pp. 134–141.

[20]Chern, J. S., Yang, C. Y., Vinh, N. X., and Hanson, J. M., "Deceleration and Heating Constrained Footprint of Shuttle Vehicles," *Acta Astronautica*, Vol. 12, No. 10, 1985, pp. 819–829.

[21]Kondratyev, K. Y., and Hunt, G. E., *Weather and Climate on Planets*, Pergamon, Oxford, England, UK, 1982.

[22]Seiff, A., "Atmospheres of Earth, Mars and Venus, as Defined by Entry Probe Experiments," *Journal of Spacecraft and Rockets*, Vol. 28, No. 3, 1991, pp. 265–275.